Published in final edited form as:
Cell Tissue Res. 2011 June ; 344(3): 415–433. doi:10.1007/s00441-011-1173-y.

Cell proliferation and cytoarchitectural remodeling during spinal cord reconnection in the fresh-water turtle *Trachemys dorbignyi*

María Inés Rehermann,
Departamento de Neurofisiología Celular y Molecular, Avenida Italia 3318, Montevideo, Uruguay

Federico Fernando Santiñaque,
Servicio de Clasificación Celular y Citometría de Flujo, Instituto de Investigaciones Biológicas Clemente Estable (IIBCE), Avenida Italia 3318, Montevideo, Uruguay

Beatriz López-Carro,
Servicio de Clasificación Celular y Citometría de Flujo, Instituto de Investigaciones Biológicas Clemente Estable (IIBCE), Avenida Italia 3318, Montevideo, Uruguay

Raúl E. Russo, and
Departamento de Neurofisiología Celular y Molecular, Avenida Italia 3318, Montevideo, Uruguay

Omar Trujillo-Cenóz
Departamento de Neurofisiología Celular y Molecular, Avenida Italia 3318, Montevideo, Uruguay

Omar Trujillo-Cenóz: omar@iibce.edu.uy

Abstract

In fresh-water turtles, the bridge connecting the proximal and caudal stumps of transected spinal cords consists of regenerating axons running through a glial cellular matrix. To understand the process leading to the generation of the scaffold bridging the lesion, we analyzed the mitotic activity triggered by spinal injury in animals maintained alive for 20–30 days after spinal cord transection. Flow cytometry and bromodeoxyuridine (BrdU)-labeling experiments revealed a significant increment of cycling cells around the lesion epicenter. BrdU-tagged cells maintained a close association with regenerating axons. Most dividing cells expressed the brain lipid-binding protein (BLBP). Cells with BrdU-positive nuclei expressed glial fibrillary acidic protein. As spinal cord regeneration involves dynamic cell rearrangements, we explored the ultra-structure of the bridge and found cells with the aspect of immature oligodendrocytes forming an embryonic-like microenvironment. These cells supported and ensheathed regenerating axons that were recognized by immunocytological and electron-microscopical procedures. Since functional recovery depends on proper impulse transmission, we examined the anatomical axon-glia relationships near the lesion epicenter. Computer-assisted three-dimensional models revealed helical axon-glial junctions in which the intercellular space appeared to be reduced (5–7 nm). Serial-sectioning analysis revealed that fibril-containing processes provided myelinating axon sheaths. Thus, disruption of the ependymal layer elicits mitotic activity predominantly in radial glia expressing BLBP on the lateral aspects of the ependyma. These cycling cells seem to migrate and contribute to the bridge providing the main support and sheaths for regenerating axons.

Correspondence to: Omar Trujillo-Cenóz, omar@iibce.edu.uy.

Keywords

Spinal cord; Cell proliferation; Regeneration; Radial glia; Re-myelination; Turtle; *Trachemys dorbignyi* (Chelonia)

Introduction

Anamniotes such as cyclostomes (Rovainen 1976; Wood and Cohen 1979; Armstrong et al. 2003; Shifman et al. 2007), certain fish (Coggeshall and Youndblood 1983; Dervan and Roberts 2003; Takeda et al. 2007; Reimer et al. 2008), anuran larvae (Lorente de Nó 1921; Michel and Reier 1979; Beattie et al. 1990; Gibbs and Szaro 2006), and tailed amphibians (Piatt 1955; Butler and Ward 1965; Stensaas 1983; Davis et al. 1990; Chevallier et al. 2004; Mchedlishvili et al. 2007) are able to repair their damaged spinal cords and to recover some of the functions lost by injury. In addition, we have recently reported that an amniote vertebrate (the fresh-water turtle, *Trachemys dorbignyi*) also exhibits outstanding self-repairing capabilities after the complete transection of the spinal cord. Turtles spontaneously reconnect their severed spinal cords, leading in some cases to substantial motor recovery (Rehermann et al. 2009). The same study has revealed the occurrence of regenerated axons traveling on a cellular scaffold bridging the injured spinal cord segments. In contrast to mammals, reactive glial cells in turtles do not form the typical “glial scar” blocking the passage of incoming axons (Ramón y Cajal 1913–1914; Silver and Miller 2004; Thuret et al. 2006). The present work focuses on the following: (1) the reconnection of the transected cord mediated by axonal regrowth and cell proliferation, (2) the identification of the origin of some of the regenerating axons, (3) an assessment of the spatial spread of the mitotic wave elicited by spinal cord transection, (4) the nature of the proliferating cells facilitating axonal growing, and (5) a study of the early steps of the remyelination process that occurs during repair.

Transection of the spinal cord and the concomitant retraction of the rostral and caudal stumps create a gap that is initially filled by a clot. This is replaced later by a cellular bridge supporting the transit of the regenerating axons (Rehermann et al. 2009). The development of this cellular scaffold should involve active cell proliferation and cell migration toward the damaged site. Since spinal cord injuries trigger mitotic activity in the cord parenchyma (Adrian and Walker 1962; Liu et al. 1998, 2000; Mothe and Tator 2005; Vessal et al. 2007; Meletis et al. 2008), we hypothesize that the injured site should contain a large number of cycling cells in close association with the regenerating axons. To test this hypothesis, we have employed two technical approaches: (1) the quantification of dividing cells by flow cytometry (FC), and (2) the quantification of bromodeoxyuridine (BrdU)-tagged cells in sections obtained at various spinal cord levels. We have also determined the nature of the cycling cells by double-labeling immunocytochemical experiments in BrdU-injected turtles.

Spinal cord regeneration involves processes such as the replacement of lost cells, axonal growth with navigation toward proper targets, and remyelination (Horner and Gage 2000; Thuret et al. 2006). These diverse events normally occur dynamically during the development of the central nervous system (Sanes et al. 2006). We thus hypothesize that, during endogenous repair of the turtle spinal cord, an embryonic-like environment appears in the healing zone. During this process, regenerating axons have to be myelinated if they are to conduct rapid signals for an efficient functional recovery (Horner and Gage 2000). This does not exclude the regeneration of non-myelinated axons that, for example, might contribute to the restoration of important vegetative functions. To analyze the microenvironment surrounding the regenerating axons at the bridge level and the early myelination process, we have taken advantage of the high resolution offered by transmission

electron microscopy (TEM) complemented with computer-assisted three-dimensional (3D) models. The TEM data show a loose cellular organization that differs from the compact histological architecture characteristic of the undamaged spinal cord. Within this embryonic-like microenvironment, we have found diverse stages of ensheathing that range from partially covered axons to complete sheaths with multiple myelin layers. In line with our previous results (Rehermann et al. 2009), these are the first reports that, in an amniote vertebrate, new cells are incorporated into the disrupted spinal cord region creating a suitable microenvironment for the displacement of target-searching glial processes in parallel with axonal regrowth.

Materials and methods

Animals

Fresh-water turtles (*Trachemys dorbignyi*, with carapace lengths ranging between 5–12 cm; *n*=27) were maintained in temperate aquaria (28–30°C) under natural illumination and fed daily with small earthworms. The selected temperature optimizes turtle feeding behavior and also promotes cell proliferation (Radmilovich et al. 2003). All the studies were conducted under the guidance of our local Committee for Animal Care and Research following NIH guidelines for the maintenance and use of laboratory animals (CHEA, UDELAR).

Surgical procedures

The relevant surgical procedures have been described in detail elsewhere (Rehermann et al. 2009). Briefly, turtles were sedated with ketamine chlorhydrate (40 mg/kg body weight) and deeply anesthetized with isofluorane (Forane, Abbott Laboratories, Berkshire, UK). The third dorsal scute was then partially removed to expose the underlying spinal cord, which was transversally cut at the level of the 13th–14th thoraxic (from the 1st cervical vertebra) vertebrae with a fine scalpel. Completeness of the section was checked by observing the immediate retraction and separation of both spinal stumps with diameters ranging between 250 and 300 μm. The space between the resulting stumps was about 0.1 mm (based on measurements of the clot width). Histological evidence indicating the efficacy of the surgical procedure was as previously presented (Rehermann et al. 2009, Fig. 1). Finally, the lifted scute was replaced and glued with cyanoacrylate. We also performed “sham” experiments in which the spinal cord was exposed but not injured (*n*=3). Despite the paralysis of the hindlimbs, the animals were able to catch living prey and did not require special postoperative care. All operated animals (*n*=19) were maintained in temperate aquaria (25°C) and fed with living earthworms. All experiments were carried out on animals maintained alive for 20–30 days after spinal cord transection. We selected this time window because previous studies (Rehermann et al. 2009) had indicated that the bridge connecting the caudal and cephalic stumps had developed, and that the majority of injured turtles had started to show movements (still uncoordinated) of their hindlimbs.

Flow cytometry

Spinal cord portions of 3–4 mm in length were obtained from homologous regions of control animals (*n*=3), sham-experimented turtles (*n*=3), and injured turtles (*n*=3) were washed in phosphate-buffered saline (PBS) and disaggregated in 400 μl PBS by chopping with a razor blade. The cell suspension was then filtered through a 45-μm nylon mesh to remove tissue debris. Cells were fixed drop by drop with 1 ml fresh ice-cold ethanol (70% absolute ethanol, 30% filtered PBS) by using a vortex to avoid the formation of cell clumps. Within 24–48 h after fixation, the cell suspension was centrifugated at 1200 rpm for 6 min and resuspended in 250 μl PBS after discarding the supernatant. For DNA staining, 25 μl propidium iodide (PI; 1 mg/ml; Sigma) was added to the cell suspension with 25 μl RNase A

(1 mg/ml; Sigma) to avoid the staining of double-stranded RNA. Samples were kept on ice for 10 min and immediately analyzed by FC.

A FACSVantage flow cytometer (Becton Dickinson [BD], San José, USA) equipped with a water-cooled argon ion LASER Innova 304 (Coherent, USA) tuned to emit at 488 nm was used. The laser power was set to 100 mW, and the fluorescence emitted from PI was collected in FL2 by using a 575/26 band-pass filter. A 70-μm nozzle was selected to perform flow cytometric measurements. To optimize fluorescence detection and to check instrument linearity, we used chicken red blood cells and DNA QC particles (BD). Forward scatter (FSC-H), side scatter (SSC-H), pulse-area or total emitted fluorescence (FL2-A), and pulse-width or duration of fluorescence emission (FL2-W) were analyzed with CELLQuest software (BD). Dot plots of FL2-A versus time were used as a control of fluorescence emission during sample analysis. A total of 5000 events were analyzed per sample. Doublets were excluded from the analysis through gating on the G1, S, and G2 cell populations (R1) in FL2-A versus FL2-W dot plots. The relative proportion of cells in S and G2 phase was estimated in a FL2-A histogram based on R1 gated data by using appropriate markers (M1=G1 and M2=S+G2/M).

BrdU injection and immunocytochemistry

Turtles with injured cords (*n*=3) began to receive intraperitoneal BrdU injections 20 days after surgery. They were injected during 3 consecutive days (daily injections of 100 mg kg body weigth), anesthetized as described, and fixed by perfusion on the fourth day. Uninjured control turtles (*n*=3) also received the same BrdU doses and were anesthetized and fixed by perfusion on the fourth day. Fixed spinal cords from turtles injected with BrdU were dissected out and divided into separated portions of 4 mm in length. To maintain an ordered cephalic-caudal arrangement of the partitioned cord, we made asymmetric cuts in the cephalic and caudal surfaces of each portion. The region comprising the damaged cord was identified as the lesion epicenter (LEPI), because of its more transparent appearance as viewed under the dissection microscope. The LEPI was considered as a landmark separating rostral from caudal segments (RS-CS). The spinal cords were serially cut (70 μm thickness) with a vibrating microtome, and the floating sections were sequentially collected in numbered plastic wells. Twenty sections were randomly selected from LEPI and 10 sections from both adjacent RS and CS. BrdU detection was performed as follows: the sections were pretreated with 2 N HCl, washed several times with phosphate buffer (PB), and incubated overnight with the BrdU antibody. For quantitative studies, the secondary antibody was conjugated with horseradish peroxidase and processed with 3,3′-diaminobenzidine. For double-staining experiments, secondary antibodies were conjugated with appropriated fluorophores.

For other immunohistochemistry studies (*n*=4), tissues were sectioned with a vibrating microtome (at 60–80 μm). Sections were placed in PB with 0.5% bovine serum albumin (BSA) for 30 min and then incubated with the primary antibodies diluted in PB with 0.3% Triton X-100 (Sigma-Aldrich). Incubation times and antibody concentrations were optimized for each case. After being washed in PB, sections were incubated in secondary antibodies conjugated with various fluorophores. In co-labeling experiments, Alexa 488 and 633 (Invitrogen) were used to avoid cross-talk. We carried out controls by suppressing primary antibodies during tissue processing.

To immunophenotype dividing cells and to label the growing axons, we assayed various antibodies as shown in Table 1.

Unspecific sites were routinely blocked with BSA (0.5%), and then sections were incubated overnight with the primary serum (in PB and 0.3% Triton-X 100). After being washed, the

sections were incubated with the secondary antibodies (1:200–1:1000). Control experiments were carried out by replacing antibodies with preimmune serum.

Axonal tracers

To identify the origin of the regenerating axons crossing the lesion, we used two technical procedures involving fixed and living tissues. In some experiments, we applied 1,1′, di-octadecyl 1–3,3,3′,3′-tetramethylcarbocyanine perchlorate (DiI; Invitrogen) crystals to fixed tissues (Godement et al. 1987; Köbbert et al. 2000), specifically to the sensory nerves entering the cord rostral to the lesion site. At the anterior limit of the third scute (vertebral segments 11th–12th), the spinal ganglia and sensory nerves are more accessible than at other levels, and hence spurious labeling would be more difficult to avoid. In other experiments, the same lipophilic dye was applied to the cut surfaces of the cord 3–4 mm caudal to the lesion site. Experiments involving living animals were performed by pressure-injecting neurobiotin (Vector Labs, Burlingame, Calif., USA; SP-1120-Lot no. 1106) into the caudal portions of the cord (15th–16th segments) in spinal-transected turtles.

As shown in Fig. 1, the incoming sensory nerves are easily accessible away from their entrance into the ganglia. To reduce the risk of spurious labeling when applying DiI to the cut surface of the cord, we carried out experiments in which the sectioned surface was maintained within the vertebral canal and covered with an ultrathin film of Polyvinyl Formvar (Polysciences, Warrington, Pa., USA) supported on Sjöstrand-type rings (Sjöstrand 1967); this film remained attached to the cord and formed a continuous coat. The film was then pierced with a fine glass needle, and DiI crystals were deposited on the perforated spot. By this means, direct contact of the tracer and tissues was limited to the small area underlying the opening made in the film coat (Fig. 2a). To avoid the potential spread of DiI outside the desired target during incubation, the region was covered with a second film that firmly stuck to the first. Labeled samples were transferred to a 4% paraformaldehyde/PBS solution and placed in the dark at 37°C for 20 days. After incubation, the film was removed with a pair of fine tweezers, and the pieces were embedded in a mixture of albumin and gelatin, hardened with glutaraldehyde, and sectioned with a vibrating microtome.

We also performed “in vivo” experiments to identify retrogradely labeled neurons. A neurobiotin solution (10 mM in saline; Vector Laboratories, Burlingame, Calif., USA) was pressure injected (Picospritzer III, Parker Instrumentation) with a glass micropipette placed within the caudal stumps of the spinal cord 20–30 days following injury (Fig. 2b). At 4 days after injection, the animals were fixed by perfusion, and the spinal cord was sectioned with a vibrating microtome. To reveal the presence of retrogradely labeled neurons in segments cephalic to the lesion site, the sections were incubated in a 0.5% BSA solution for 1 h, washed in PBS several times, and transferred to a 1/400 solution of streptavidin conjugated with Alexa Fluor 633 (Invitrogen, cat. no. S21375) for 2 h. For the tracer experiments, we employed 5 turtles.

Fluorescent signals were detected by using epifluorescence or confocal microscopy (Olympus VF 300). The images were imported into Fluoview 5 (Olympus) and then exported to PhotoShop (Adobe Systems, San José, Calif., USA) or CorelDraw (Corel Corporation, Ottawa, Ontario, Canada) for cropping and the creation of figure montages. When considered pertinent, the preparations were also viewed under Nomarsky optics. The images recorded with the confocal microscope were single optical sections and stacks resulting from the superposition of multiple optical sections. Transverse images of the stacks following the *x*-*z* and *y*-*z* planes were obtained with FluoView 5 (Olympus). When making stacks, we followed the data provided by the software to adjust spacing along the *z* axis and the diameter of the pinhole.

TEM procedures

For TEM studies (n=3), the spinal cords of anesthetized turtles were fixed by perfusion in an aldehyde mixture containing 4% paraformaldehyde and 1% glutaraldehyde dissolved in 0.1 M PB (pH 7.4). Small spinal cord portions were washed several times in PB and post-fixed in 1% OsO_4 dissolved in the same buffer. The pieces were dehydrated and embedded in Durcupan ACM. Series of ultrathin sections were mounted on Formvar-coated slot grids (2×1 mm) and contrasted with uranyl acetate and lead citrate. The material was examined with a Jeol CX electron microscope equipped with a 4000 AM DVC digital camera. All 3D representations were obtained with the BioVis program (www@biovos3d.com) based on images obtained from continuous series of ultrathin sections.

Quantification and statistical analysis

For a comparison of cell proliferation in control, sham-injured, and injured spinal cords as shown by FC, a non-parametric one-sided Wilcoxon test was used. A value of $P< 0.05$ was considered statistically significant.

To estimate the number of BrdU-tagged nuclei, we followed the guidelines proposed by Guillery and Herrup (1997). We counted the labeled nuclei enclosed within a circle (150 μm radius) centered on the central canal (CC). Counts were further processed by applying the Abercrombie correction (Abercrombie 1946). The same protocol was employed to estimate the number of BrdU-tagged nuclei in control experiments. In these cases, we identified, as topologically equivalent to LEPI, the spinal cord region (4 mm long) underlying the third scute. Distribution profiles of both injured and control animals were generated by plotting the Abercrombie-corrected data obtained from each section level (y axes) versus distances (measured in micrometers) from the lesion site (x axes). The significance of the differences between injured and control animals was estimated by applying the Kruskal-Wallis and the Wilcoxon pair-wise non-parametric tests (for details, see Results).

Results

Regenerating axons “bridge” injured site

To confirm that the amputated axons were able to regenerate and to cross the lesion site, we employed immunocytochemical and axon-labeling procedures. As shown in Fig. 3a, at 20 days after spinal cord transection, nerve fibers positive for Neurofilament M (NF-M) had crossed the injured site. At the tips of some of these fibers, we found the typical growth cones described by Ramón y Cajal (1913–1914) in the injured spinal cord of the different mammals. As in the regenerating spinal cord of cyclostomes (Shifman et al. 2007) and tadpoles (Lorente de Nó 1921), these growth cones adopted the form of cylindroconical masses or lanceolated endings without conspicuous filopodia (Fig. 3bc). The morphology of these growth cones was less elaborate than that reported for growth cones in the developing spinal cord of *Xenopus* tadpoles (Nordlander 1987). We also observed small terminal “rings” (Fig. 3c, d) reported to occur during axonal sprouting in the injured central nervous system (Ramón y Cajal 1913–1914) or in some synaptic contacts (Gray and Guillery 1961; Novotny 1979). To confirm the occurrence of growth cones, we performed TEM studies. Consistent with previous work (Tennyson 1970; Landis 1983; Williams et al. 1988), our images revealed that the bulbous tips of sprouting axons contained numerous clear-core vesicles together with a small number of “coated vesicles”. The vesicular material was intermingled with fine disorganized thin fibrils (Fig. 3d–f).

The zone that contained growing axons also exhibited some of the classical “retraction balls” of Ramón y Cajal (1913–1914) or dystrophic nerve bulbs. This other kind of axonal compartment was larger than growth cones and tended to exhibit a spherical shape (Fig. 3g).

When examined with TEM (Fig. 3h), these end bulbs were recognized not only by their larger size, but also by fine structural details such as the presence of a neurofibrillar core, sparse dispersed dense-core vesicles, and large electron-dense phagosomes (Williams et al. 1988). More recent investigations support the view that these enlarged terminals are metabolically active axons in the stand-by mode (Li and Raisman 1995; Houle and Jin 2001) and not decaying nerve fibers as originally proposed by Ramón y Cajal (1913–1914).

Axon-labeling experiments employing DiI and neurobiotin (Huang et al. 1992) provided information about the origin of some of the crossing fibers (Fig. 4a). When DiI crystals were applied to the tips of sectioned sensory nerves close to dorsal ganglia that lay rostral to the injured zone, sensory neurons in the ganglia (Fig. 4b) and the entering axons (Fig. 4c) appeared stained at various levels of the cord. Labeled axons were recognized at the bridge region and also within the caudal stump (Fig. 4d). Double-labeling experiments with NF-M antibody revealed DiI-stained axons running between neurons caudal to the lesion site (Fig. 4e). In a previous paper, we have described synaptic-like contacts between regenerated sensory fibers and spinal cord neurons (Rehermann et al. 2009). These results are consistent with the recognized regeneration overcapabilities of the dorsal root axons (Ramón y Cajal 1913–1914; Davies et al. 1999). We obtained robust staining of crossing axons when DiI crystals were applied to the cut surface of the cord in regions caudal to the injured site (Fig. 4f, g). Moreover, some of the parent perikarya were depicted in regions rostral to the lesion site by retrograde diffusion of the dye along the axonal membranes (Fig. 4h). As reported previously (Rehermann et al. 2009), DiI-stained neurons were commonly of a small size and appeared to form assemblies distributed at various levels of the rostral stump. Thorough low power exploration of the mesenchymal sheaths covering the regenerating bridge showed no evidence of “dye bleeding” toward the regenerating axon bundles. In addition, high magnification confocal images revealed the specific staining of axons of diverse diameters without evidence of dye transport via the extracellular space (Fig. 4g). Low power images covering several cord segments also indicated that the meninges were free from dye labeling, thus making spurious stain originating from this source unlikely. These experiments indicated that some of the regenerating axons originated from sensory collaterals running along the dorsal funiculi and also from medium-sized interneurons lying close to the injured region. Additional evidence resulted from “in vivo” experiments involving the retrograde transport of neurobiotin. These experiments confirmed that small and medium-sized neurons, located close to the injured site, were one of the sources of regenerating axons. Using this technical approach (Huang et al. 1992), we found Golgi-like and granular stained neurons (Fig. 5a). Abundant Golgi-like labeled processes occurred near the stained neuron pools (Fig. 5b, arrows).

Newborn cells for repairing injured spinal cord

In the spinal cord of the turtle, substantial cell proliferation occurs in the ground state (Fernández et al. 2002; Russo et al. 2008). To investigate whether the number of cycling cells was affected by spinal injury, the cell cycle profile was examined by measuring the DNA content of PI-stained cells by FC. Typical examples comparing normal uninjured turtles, sham experiments, and spinal-transected animals are illustrated in Fig. 6, Table 2. The distribution of cells in the three cycle phases showed a significant increment of cycling cells in the injured animals. The increment was statistically significant ($P<0.05$, one-sided Wilcoxon rank-sum test) at LEPI without statistically significant differences at more rostral or caudal levels.

To study the spatial extension of the increased cell proliferation, we performed “fine grain” experiments in which S-phase cells were BrdU-stained, and the number of BrdU-tagged nuclei were estimated at various spinal cord levels. This technical approach with various fluorophores allowed double-labeling experiments for the identification of the nature of the

cycling cells and their relationships with the regenerating axons. As in the FC experiments, we found, at the LEPI level, a statistically significant increase in the number of BrdU-positive nuclei in the injured animals compared with control animals (Fig. 7a). The Kruskal-Wallis test showed that independent samples from three injured turtles (20 samples each group) came from distributions with equal medians. The same test showed that control turtles (n=3, 20 samples each group) also had distributions with equal medians. The Wilcoxon test between injured and control turtles revealed that medians were significantly different (P<0.000001). However, differences between injured and control animals attenuated dramatically at more cephalic or caudal portions of the cord. At these levels, Wilcoxon pair-wise tests (Bonferroni correction) demonstrated that the number of labeled nuclei in the injured animals was significantly larger than that in controls (P<0.05) only in seven out of nine pair-wise comparisons (in both rostral and caudal segments).

Analysis in the transverse plane showed BrdU-labeled cells throughout the spinal parenchyma (Fig. 7b, c) with concentrations of labeled nuclei around the CC (Fig. 7d). BrdU-tagged nuclei were evenly stained or exhibited dark granules in contrast to the pale nuclear background (not shown). Examination at the light-microscope level also revealed typical mitotic figures (Fig. 7e) that were confirmed by employing TEM procedures in injured but not BrdU-injected turtles (Fig. 7f). To determine the relationship between the cycling cells and the pathways of regenerating axons, we performed double-labeling experiments with an axon-marking antibody (NF-M). As shown in Fig. 7g, h, NF-M-positive axons travelled through the bridge region associated with cells exhibiting BrdU-positive nuclei. The exploration of orthogonal planes (x-z and y-z axes) obtained from optical stacks revealed a close association between the nerve fibers crossing the injured region and cycling cells (Fig. 7h). This intimate relationship between cells in the bridge and the crossing axons was explored in detail by employing TEM procedures (see below).

Molecular phenotypes of cycling cells

To identify the molecular phenotypes of cycling cells, we performed double-labeling experiments employing glial and neuronal markers. The use of brain lipid-binding protein (BLBP) antibody (Feng et al. 1994) indicated robust double-labeling of BrdU-positive cells (Fig. 8a). In addition, the low power images illustrated the lax organization of the cells expressing BLBP, a feature consistent with our TEM findings (see below). Analysis of the tissues at higher magnification confirmed unambiguously that some of the cells expressing BLBP had incorporated BrdU (Fig. 8b–d).

A different picture resulted from the use of glial fibrillary acidic protein (GFAP) antibody. GFAP expression was mainly restricted to cell processes with few identifiable cell bodies (Reichenbach and Wolburg 2005). Therefore, reliable assessment of double-labeling was a difficult task. However, we were able to identify a few cell bodies expressing GFAP and containing BrdU-labeled nuclei (Fig. 8e–g). In the bridge region, none of the BrdU-positive cells expressed the neuronal marker, anti-human neuronal protein (not shown). Disregarding the bias that might have been introduced by difficulties in identifying the cell bodies of GFAP-positive cells, our prevalent view is that most proliferating cells expressed BLBP.

Cytoarchitecture of the bridge: an embryonic-like environment

In contrast to the usual compact cell organization found in both the gray and white matter of the spinal cord, the bridge was characterized by a loose arrangement of cells and axons. Bridge cells formed a scaffold supporting and enveloping bundles of regenerating axons (Fig. 9a). The more abundant cells shared characteristics of fibril-containing glia and the axon-ensheathing properties of oligodendrocyte-lineage cells. In cross sections, they exhibited a polymorphic appearance with multiple processes stemming from the perinuclear

cytoplasm. We have previously reported that, in turtles, typical radial glia (RG) are present with their processes filled with compact bundles of fine fibrils (Trujillo-Cenóz et al. 2007). Interestingly, cells with characteristics of a "hybrid oligodendrocyte/RG antigenic phenotype and a RG morphology" have been described in rats (Choi et al. 1983; Choi and Kim 1985; Hirano and Goldman 1988; Fogarty et al. 2005). The mechanical stability of the cell scaffold seems to be mediated by multiple intercellular contacts (Fig. 9a, arrows), some of which exhibit the fine structural characteristics of desmosomes (Fig. 9e). Additional cytoskeleton strength might be provided by compact bundles of gliofibrils present in most glial processes.

Small and medium-sized regenerating axons appeared encased within infolds of the cell plasma membrane or covered by several glial lamellae containing gliofibrils (Fig. 9c, d). Similarly, neural processes "enclosed with fascicles formed by ependymal processes" have been described by Michel and Reier (1979) in *Xenopus laevis* tadpoles during early regeneration of the transected spinal cord. To examine in detail the anatomical axon-glial relationships, we generated 3D models based on TEM images obtained from uninterrupted series of ultrathin sections (Fig. 9f). The models revealed that, at this stage, most of the regenerating axons were loosely covered by discontinuous glial membranes. Together with the usual axon-glia spacing (20 nm wide), more intimate axon-glia junctions were present characterized by an increased electron density and a reduced periaxonal space of 5–7 nm in width (Fig. 10a, b). The 3D models revealed that these electron-dense junctions were not continuous but formed irregular helical bands extending along the ensheated axon (Fig. 10c, arrowheads in 3D models). Serial section analysis also showed that axon-enveloping could be initiated from a glial cell prolongation containing bundles of gliofilaments (Fig. 11a, b) similar to those of RG. TEM images and the resulting 3D model (Fig. 11e) revealed the spatial progress of ensheating. The example illustrated in Fig. 11 shows the starting point of the enveloping process with a small axon-glial contacting area (Fig. 11a) and the fully ensheathed axon with the familiar multilamellar myelin organization at the end of the series (Fig. 11c, d). Notably, the dense helicoidal junctions remained present, even at this more advanced myelination stage (Fig. 11g).

Discussion

Amputated axons regenerate and bridge the transected cord

The experiments described in this paper are in agreement with previous findings indicating that freshwater turtles are able to attain the neural reconnection of the severed cord (Rehermann et al. 2009). We also present compelling evidence that regenerating axons originate from two main sources: (1) sensory fibers arising from the dorsal root ganglia and (2) axons from propiospinal interneurons lying close to the lesion site in the rostral stump. Our results suggest that axons stemming from neurons of higher centers do not make a major contribution to the early reconnection process. However, the time window used in our experimental approach cannot exclude the possibility that axons from higher centers might cross the lesion site at later stages, reconnecting them with spinal neurons. Reactivation of anatomically circumscribed circuits close to the lesion site by regrowth of sensory axons seems to play a crucial role during spinal cord reconnection. We have found evidence that sensory axons originating from cephalic portions of the cord cross the lesion site. However, the contribution of axonal regrowth from sensory fibers arising from caudal ganglia is also possible. Application of axonal tracers emitting light at different wavelengths in sensory nerves caudal and rostral with respect to the lesion site might help to solve this issue.

The regeneration capabilities of turtles appear limited when compared with those of anuran tadpoles in which mesencephalic and rhombencephalic neurons are retrogradelly labeled after spinal cord regeneration (Gibbs and Szaro 2006). We should keep in mind, however,

that functional recovery in turtles is incomplete, because injured animals are able to recover stepping but not normal swimming (Rehermann et al. 2009). Nonetheless, our findings support the view that the regenerative capacities of the spinal cord are not exclusive to anamniotes and remain, even though restricted, in some post-natal amniotes.

Injury increases mitotic activity

In the normal uninjured spinal cord of rats, slow basal mitotic activity mainly occurs in white matter tracts. The majority of BrdU-labeled cells express glial markers (Horner et al. 2000). However, in the same animals, spinal injury induces an increment of proliferating cells. Under these circumstances, the BrdU-labeled nuclei colocalize with progenitor or glial cell markers but never with neuronal proteins (Horky et al. 2006). Surprisingly, indirect damage of the spinal cord (e.g., rhizotomy) induces not only cell proliferation, but also the generation of new neurons (Vessal et al. 2007). This suggests that different insults might activate progenitors with various lineage potentials.

A different scenario occurs in turtles. In these reptiles, mitotic activity persists, being mainly concentrated on the lateral aspects of the CC. In these regions, clusters of electrical- and dye-coupled RG occur with the molecular and physiological characteristics of cycling precursor cells (Russo et al. 2008). Our experiments employing both FC and BrdU-labeling have revealed that spinal cord transection elicits a noticeable increment in the mitotic activity of some spinal cells and that this peaks at the LEPI and decreases steeply both in the rostral and in the caudal directions. The observed cell proliferation is consistent with the formation of a cellular scaffold that supports the navigation of sprouting axonal branches, which cross the damaged region (Rehermann et al. 2009).

Nature of the cycling cells

Studies carried out on lizards (Egar et al 1970), tailed amphibians (Singer et al. 1979; Zhang et al. 2000; Mchedlishvili et al. 2007), and immature eels (Dervan and Roberts 2003) have revealed the role played by ependymal cells in the healing and reconstruction of the injured spinal cord. Our findings are, in general, coincident with these previous reports. In the turtle, BLBP-positive RG that flank the CC form clusters of cells that are electrically and metabolically coupled, incorporate BrdU, express Pax6, and display electrophysiological properties characteristic of neural progenitors (Russo et al. 2008). A plausible hypothesis is that neural injury elicits an increment of the intrinsic basal mitotic activity sustained by the lateral clusters of RG, thereby generating cells that migrate to the injured site. The capability of RG expressing BLBP to contribute to neural repair has been demonstrated in rodents in which transplanted embryonic RG “bridge spinal cord lesions and promote functional recovery” (Hasegawa et al. 2004). However, we cannot exclude as yet an alternative situation similar to that described in rats. In this rodent, the neuron/glia-type 2 antigen (NG2)-expressing progenitors appear to be vulnerable to injury, but a separate neural stem cell population is activated to replace the damaged one (Horky et al. 2006). Therefore, the cycling cells found in the injured spinal cord of turtles might belong to another non-vulnerable cell population; this population might be the one that actually initiates mitotic activity. At present, we cannot exclude the possibility that oligodendrocytes ensheathing the amputated axons or Schwann cells covering the entering sensory roots can dedifferentiate to envelope the regenerated axons within the bridge. Additionaly, the expression of RG markers such as BLBP in cells within the bridge might arise from reactive astrocytes transformed to an immature state (Shibuya et al. 2003; Iseda et al. 2004). However, the fine structural evidence indicates a predominance of gliofibrill-containing cells covering the sprouting axons, thus suggesting a RG origin.

Since turtles exhibit neural reconnection and partial motor recovery, it is pertinent to ask how the proliferating niches are remodeled after injury. This issue has been investigated in rats by using retrovirus technology to target NG2-expressing cells (Sellers et al. 2009) but remains unexplored in turtles. In addition to BLBP-positive cells, some GFAP-positive cells also appear with BrdU-stained nuclei. However, since the most robust expression of the protein occurs in their fine processes (Reichenbach and Wolburg 2005), an evaluation of the contribution of the GFAP-positive cells to the total population of cycling cells is difficult.

Cytoarchitectural remodeling during neural reconnection

The zone bridging the disrupted spinal cord exhibits a peculiar structure with loose intercellular contacts and an enlarged extracellular space, all of which resemble embryonic cell organization. In this respect, our TEM images are similar to those published by Singer et al. (1979) in the regenerating cord of the newt. The cytoarchitecture and the abundance of finger-like processes and lamellae suggest a highly dynamic scenario. Indeed, recent “in vivo” studies performed in developing zebrafish have provided compelling evidence that oligodendrocyte progenitors move actively and send processes back and forth to reach and recognize their relevant axon targets (Kirby et al. 2006). Moreover, highly motile growth-cone-like structures have been observed in cultured post-migratory premyelinating oligodendrocyte (Fox et al. 2006). In turtles, cells belonging to the bridge matrix also behave as oligodendrocyte precursors and/or premyelinating oligodendrocytes (Levine et al. 2001) enveloping regenerating axons. Then, analogous dynamic phenomena most probably occur in the embryonic-like microenvironment supporting neural repair in the turtle spinal cord.

In view of the structural similarities between the regenerating spinal cord and the embryonic tissues, we can pertinently discuss the regeneration potentialities of the spinal cord at various developmental stages. For example, during the development of the chick spinal cord, the effects of spinal injury are known to change from successful to unsuccessful repair and recovery around embryonic day 13 (E13; Ferretti and Whalley 2008). Taking advantage of the facilities offered by this classical model, and using fluorescent tracing labels, Hasan et al. (1993) have established that, following complete transection in the later stages of the “permissive period” (E10–13; Keirstead et al. 1992), spinal cord repair is increasingly attributable to true axonal regeneration and not to developmental regulation (for a discussion, see Ferretti and Whalley 2008).

The end of the permissive period has been associated with the onset of myelination, since its delay (by injection of a monoclonal antibody against a galactocerebroside) results in complete neuroanatomical repair and functional recovery. This occurs even if the spinal cord is severed as late as E15 (Keirstead et al. 1992). In turtles, the permissive period has been extended to the postnatal period and seems to be independent of the myelination process. However, an exploration of the possibility that antibodies against myelin might affect the repairing process in the turtle should be of interest.

In regenerating spinal cords of turtles, the analysis of a series of sections has indicated that the axon-glial anatomical relationships range from simple small areas of contact to thick complete cytoplasmic envelopes surrounding the regenerating axons. Two issues are worth discussing here. The first is concerned with the presence of electron-dense junctions distributed along the periaxonal space. High magnification images have revealed that, in these junctions, the extracellular space appears to be dramatically reduced, as occurs in gap junctions. Nevertheless, the functional significance of these axon-glial junctions is unclear. Gap junction coupling via Cx43 and Cx26 is important for the regulation of a variety of cellular events during cortical development (Bittman et al. 1997; Bruzzone and Dermietzel 2006; Elias et al. 2007). If gap-junction-like structures in the bridge are fully functional, they might represent a key pathway for electrical and metabolic signaling between regenerating

axons and oligodendrocyte-like cells. In turtles, we have previously determined that both Cx26 and Cx43 are expressed around the CC in which the BLBP domains of precursors are located (Russo et al. 2008). Interestingly, during development, both Cx26 and Cx43 have recently been demonstrated to have a role as adhesion molecules critical for the migration of newborn neurons along RG processes (Elias et al. 2007). Therefore, the dense junctions might represent points of anchorage for the movement of ensheating processes around regenerating axons. Our 3D models have shown that these areas of intimate contact are discontinuous and helically distributed along the axon axis. This may reflect a helicoidal movement of the glial cell during the ensheating processes. An alternative explanation for these junctions is that they might be the earliest evidence of the transverse bands that have been found in paranodal regions of mature myelinated axons and that behave, in peripheral nerve fibers, as paracellular barriers to solute flow (Hall and Williams 1971). In peripheral nerves, a major transition in the molecular phenotype of Schwann cells is believed to be driven by signals from the axons, with these, in turn, being remodeled by signals from the enveloping glia (Salzer 2003; Simons and Trotter 2007). Immunoelectron microscopy should help to resolve the nature of these enigmatic gap-junction-like structures between ensheating cells and regenerating axons.

The second issue deals with the myelination properties exhibited by gliofibril-containing cells. Our 3D studies indicate that gliofibril-containing processes are able to produce myelin lamellae like those generated by olygodendrocytes. This is in agreement with previous evidence from rodents indicating that spinal cord RG can give rise to oligodendrocytes (Choi et al. 1983; Choi and Kim 1985; Hirano and Goldman 1988).

Concluding remarks

Overall, our findings indicate that spinal cord injury elicits cell proliferation, particularly in cells expressing BLBP and GFAP. Because BLBP-positive cells on the lateral aspects of the CC maintain mitotic activity (Russo et al. 2008), they might be the main source of BLBP/BrdU-positive cells found in the bridge region. Alternatively, the BLBP- and GFAP-expressing cells in the bridge zone might arise from other types of progenitor, such as those responsible for the formation of new blood vessels in the regenerating cord (Rehermann et al. 2009). The emerging picture, when comparing our data with those described for anamniotes, is that, in the latter, the ependymal layer as a whole has retained some properties of the embryonic neural tube. For example, in *Xenopus* tadpoles, a close axonal-ependymal association exists during the early stages of the regeneration process (Michel and Reier 1979), and in axolotls, the cells lining the CC regenerate the spinal cord by inducing a multipotent blastema (Schnapp et al. 2005; Tanaka and Ferretti 2009). In turtles, however, the bridge region lacks a distinguishable CC. In any case, the BLBP-positive cells of the ependymal layer appear as the most likely candidates for the abundant pre-myelinating oligodendrocytes that envelop the incoming axons. The role played by the GFAP-positive cells is unclear as yet. Nevertheless, contrasting with mammals, they do not interfere with the transit of regenerating axons but appear aligned with axon bundles. Moreover, we have not observed, in turtles, the cavitation that occurs normally in traumatized mammalian cords (particularly in chronically injured human cords; Guest et al. 2005). Therefore, turtles appear as a unique amniote model system occupying a peculiar intermediate place between the anamniotes, with complete regenerating capabilities, and mammals, with highly restricted capabilities for the restoration of damaged spinal circuitry.

Acknowledgments

This work was partly supported by FCE_2920 from ANII and grant no. R01NS048255 from the National Institute of Neurological Disorders and Stroke to R.E.R.

We thank Dr. A. Caputi for statistical advice and Mrs. G. Fabbiani for her kind and efficient technical assistance.

References

Abercrombie M. Estimation of nuclear population from microtome sections. Anat Rec. 1946; 94:239–247. [PubMed: 21015608]

Adrian EK Jr, Walker BE. Incorporation of thymidine H3 by cells in normal and injured mouse spinal cord. J Neuropathol Exp Neurol. 1962; 21:597–609. [PubMed: 14011122]

Armstrong J, Zhang L, McClelland AD. Axonal regeneration of descending and ascending spinal projection neurons in spinal cord-transected larval lamprey. Exp Neurol. 2003; 180:156–166. [PubMed: 12684029]

Beattie MS, Bresnahan JC, Lopate G. Metamorphosis alter the response to spinal transection in *Xenopus laevis* frogs. J Neurobiol. 1990; 21:1108–1122. [PubMed: 2258724]

Bittman K, Owens DF, Kriegstein AR, Lo Turco JJ. Cell coupling and uncoupling in the ventricular zone of developing neocortex. J Neurosci. 1997; 17:7037–7044. [PubMed: 9278539]

Bruzzone R, Dermietzel R. Structure and function of gap junctions in the developing brain. Cell Tissue Res. 2006; 326:239–248. [PubMed: 16896946]

Butler EG, Ward MB. Reconstitution of the spinal cord following ablation in urodele larvae. J Exp Zool. 1965; 160:47–65. [PubMed: 5220031]

Chevallier S, Landry M, Nagy F, Cabelguen JM. Recovery of bimodal locomotion in the spinal-transected salamander, *Pleurodeles waltlii*. Eur J Neurosci. 2004; 20:1995–2007. [PubMed: 15450078]

Choi BH, Kim RC. Expression of glial fibrillary acidic protein by immature oligodendroglia and its implications. J Neuroimmunol. 1985; 8:215–235. [PubMed: 2409106]

Choi BH, Kim RC, Lapham LW. Do radial glia give rise to both astroglial and oligodendroglial cells? Dev Brain Res. 1983; 8:119–130.

Coggeshall RE, Youndblood CS. Recovery from spinal transection in fish: regrowth of axons post the transection. Neurosci Lett. 1983; 38:227–231. [PubMed: 6633929]

Davis BM, Ayers JL, Koran L, Carlson J, Anderson MC, Simpson SB Jr. Time course of salamander spinal cord regeneration and recovery of swimming: HRP retrograde pathway tracing and kinematic analysis. Exp Neurol. 1990; 108:198–213. [PubMed: 2351209]

Davies JA, Goucher DR, Doller C, Silver J. Robust regeneration of adult sensory axons in degenerating white matter of the adult rat spinal cord. J Neurosci. 1999; 19:5810–5822. [PubMed: 10407022]

Dervan AG, Roberts BL. Reaction of spinal cord central canal cells to cord transection and their contribution to cord regeneration. J Comp Neurol. 2003; 458:293–306. [PubMed: 12619082]

Egar M, Simpson SB, Singer M. The growth and differentiation of the regenerating spinal cord of the lizard *Anolis carolinensis*. J Morphol. 1970; 131:131–152. [PubMed: 5425076]

Elias LA, Wang DD, Kriegstein AR. Gap junction adhesion is necessary for radial migration in the neocortex. Nature. 2007; 448:901–907. [PubMed: 17713529]

Feng L, Hatten ME, Heintz N. Brain lipid-binding protein (BLBP): a novel signaling system in the developing mammalian CNS. Neuron. 1994; 12:895–908. [PubMed: 8161459]

Fernández A, Radmilovich M, Trujillo-Cenóz O. Neurogenesis and gliogenesis in the spinal cord of turtles. J Comp Neurol. 2002; 458:293–306.

Ferretti P, Whalley K. Successful neural regeneration in amniotes: the developing chick spinal cord. Cell Mol Life Sci. 2008; 65:45–53. [PubMed: 18030420]

Fogarty M, Richardson WD, Kessaris N. A subset of oligodendrocytes generated from radial glia in the dorsal spinal cord. Development. 2005; 132:1951–1959. [PubMed: 15790969]

Fox MA, Afshari FS, Alexander JK, Colello RJ, Fuss B. Growth conelike sensorimotor structures are characteristics features of postmigratory, premyelinating oligodendrocytes. Glia. 2006; 53:563–566. [PubMed: 16355369]

Gibbs KM, Szaro BG. Regeneration of descending projections in *Xenopus laevis* tadpole demonstrated by retrograde double labeling. Brain Res. 2006; 1088:68–72. [PubMed: 16626660]

Godement P, Vanselow J, Thanos S, Bonhoeffer F. A study in developing visual system with a new method of staining neurons and their processes in fixed tissue. Development. 1987; 101:697–713. [PubMed: 2460302]

Gray EG, Guillery RW. The basis for silver staining of synapses of the mammalian spinal cord: a light and electron microscope study. J Physiol (Lond). 1961; 157:581–588. [PubMed: 13708039]

Guest JD, Ed H, Bunge RP. Demyelination and Schwann cell response adjacent to injury epicenter cavities following chronic human spinal cord injury. Exp Neurol. 2005; 192:384–393. [PubMed: 15755556]

Guillery RW, Herrup K. Quantification without pontification. J Comp Neurol. 1997; 386:2–7. [PubMed: 9303520]

Hall SM, Williams PL. The distribution of electron dense tracers in peripheral nerve fibers. J Cell Sci. 1971; 8:541–555. [PubMed: 5576085]

Hasegawa K, Yu-Wen C, Li H, Berlin Y, Ikeda O, Kane-Goldsmith N, Grumet M. Embryonic radial glia bridge spinal cord lesions and promote functional recovery following spinal cord injury. Exp Neurol. 2004; 193:394–410. [PubMed: 15869942]

Hasan SJ, Keirstead HS, Muir GD, Steeves JD. Axonal regeneration contributes to repair of injured brainstem-spinal neurons in embryonic chick. J Neurosci. 1993; 73:492–507. [PubMed: 8426225]

Hirano M, Goldman JE. Gliogenesis in the rat spinal cord: evidence for origin of astrocytes and oligodendrocytes from radial precursors. J Neurosci Res. 1988; 21:155–167. [PubMed: 3216418]

Horner PJ, Gage FH. Regenerating the damaged central nervous system. Nature. 2000; 407:963–970. [PubMed: 11069169]

Horner PJ, Power AE, Kempermann G, Kuhn HG, Palmer TD, Winkler J, Thal LJ, Gage FH. Proliferation and differentiation of progenitor cells throughout the intact adult rat spinal cord. J Neurosci. 2000; 20:2218–2228. [PubMed: 10704497]

Horky L, Galimi F, Gage F, Horner PJ. Fate of endogenous stem/progenitor cells following spinal cord injury. J Comp Neurol. 2006; 498:525–538. [PubMed: 16874803]

Houle JD, Jin Y. Chronically injured supraspinal neurons only exhibit modest axonal dieback in response to a cervical hemi-section lesion. Exp Neurol. 2001; 169:208–217. [PubMed: 11312573]

Huang Q, Zhou D, DiFiglia M. Neurobiotin, a useful neuroanatomical tracer for in vivo anterograde, retrograde and transneuronal tract-tracing and for in vitro labelling of neurons. J Neurosci Methods. 1992; 41:31–43. [PubMed: 1578900]

Iseda T, Nishio T, Kawaguchi S, Yamanoto M, Kawasaki T, Wakisaka S. Spontaneous regeneration of the corticospinal tract after transection in young rats: a key role of reactive astrocytes in making favorable and unfavorable conditions for regeneration. Neuroscience. 2004; 126:365–374. [PubMed: 15207354]

Kirby BB, Takada N, Latimer AJ, Shin J, Carney TJ, Kelsh RN, Appel B. In vivo time-lapse imaging shows dynamic oligodendrocyte progenitor behavior during zebrafish development. Nat Neurosci. 2006; 9:1506–1511. [PubMed: 17099706]

Keirstead HS, Hasan SJ, Muir GD, Steeves JD. Suppression of the onset of myelination extends the permissive period for the functional repair of embryonic spinal cord. Proc Natl Acad Sci USA. 1992; 89:11664–11668. [PubMed: 1281541]

Köbbert C, Apps R, Bechmann I, Lanciego JL, Mey J, Thanos S. Current concepts in neuroanatomical tracing. Prog Neurobiol. 2000; 62:327–351. [PubMed: 10856608]

Landis SC. Neuronal growth cones. Annu Rev Physiol. 1983; 45:567–580. [PubMed: 6342524]

Levine JM, Reynolds R, Fawcett JW. The oligodendrocyte precursor cell in health and disease. Trends Neurosci. 2001; 24:39–47. [PubMed: 11163886]

Li Y, Raisman G. Sprouts from cut corticospinal axons persist in the presence of astrocytic scarring in long-term lesions of the adult rat spinal cord. Exp Neurol. 1995; 134:102–111. [PubMed: 7672031]

Liu L, Persson J, Svensson M, Aldskogius H. Glial cell responses, complement and clustering in the central nervous system following dorsal root transection. Glia. 1998; 23:221–238. [PubMed: 9633807]

Liu L, Rudin M, Kozlova E. Glial cell proliferation in the spinal cord after dorsal rhizotomy or sciatic nerve transection in the adult rat. Exp Brain Res. 2000; 131:64–73. [PubMed: 10759172]

Lorente de Nó R. La regeneración de la médula espinal en las larvas de batracios. Trab Lab Invest Biol Univ Madr. 1921; 19:147–183.

Meletis K, Barnabé-Heider F, Carlen M, Evergren E, Tomilin N, Shupliakov O, Frisén J. Spinal cord injury reveals multi-lineage differentiation of ependymal cells. PLoS Biol. 2008; 6:e182. [PubMed: 18651793]

Mchedlishvili L, Epperlein H, Telzerow A, Tanaka EM. A clonal analysis of neural progenitors during axolotl spinal cord regeneration reveals evidence for both spatially restricted and multipotent progenitors. Development. 2007; 134:2083–2093. [PubMed: 17507409]

Michel ME, Reier PJ. Axonal-ependymal association during early regeneration in the transected spinal cord in *Xenopus laevis* tadpoles. J Neurocytol. 1979; 8:529–548. [PubMed: 553146]

Mothe AJ, Tator CH. Proliferation, migration, and differentiation of endogenous ependymal region stem/progenitor cells following minimal spinal cord injury in the adult rat. Neuroscience. 2005; 131:177–187. [PubMed: 15680701]

Nordlander R. Axonal growth cones in the developing amphibian spinal cord. J Comp Neurol. 1987; 263:485–496. [PubMed: 3667985]

Novotny GEK. Synaptic ring images after silver impregnation. Cell Tissue Res. 1979; 204:141–145. [PubMed: 393401]

Piatt J. Regeneration of the spinal cord in the salamander. J Exp Zool. 1955; 129:177–207.

Radmilovich M, Fernández A, Trujillo-Cenóz O. Environment temperature affects cell proliferation in the spinal cord and brain of juvenile turtles. J Exp Biol. 2003; 206:3085–3093. [PubMed: 12878675]

Ramón y Cajal, SR. Degeneración y regeneración de los centros nerviosos. Moya; Madrid: 1913–1914. Estudios sobre la degeneración y regeneración del sistema nervioso, TI-II.

Rehermann MI, Marichal N, Russo RE, Trujillo-Cenóz O. Neural reconnection in the transected spinal cord of the freshwater turtle *Trachemys dorbignyi*. J Comp Neurol. 2009; 515:197–214. [PubMed: 19418545]

Reichenbach, A.; Wolburg, H. Astrocytes and ependymal glia. In: Kettenmann, H.; Ransom, BR., editors. Neuroglia. Oxford University Press; New York: 2005. p. 19-35.

Reimer MM, Sörensen I, Kuscha V, Frank RE, Liu C, Becker C, Becker T. Motor neuron regeneration in adult zebrafish. J Neurosci. 2008; 28:8510–8516. [PubMed: 18716209]

Rovainen CM. Regeneration of Müller and Mauthner axons after spinal cord transection in larval lampreys. J Comp Neurol. 1976; 168:545–554. [PubMed: 939822]

Russo RE, Reali C, Radmilovich M, Fernández A, Trujillo-Cenóz O. Conexin 43 delimits functional domains of neurogenic precursors in the spinal cord. J Neurosci. 2008; 28:3298–3309. [PubMed: 18367597]

Salzer JL. Polarized domains of myelinated axons. Neuron. 2003; 40:297–318. [PubMed: 14556710]

Sanes, DH.; Reh, TA.; Harris, WA. Development of the nervous system. 2. Elsevier/Academic Press; San Diego: 2006.

Schnapp E, Kragl M, Rubin L, Tanaka E. Hedgehog signaling controls dorsoventral patterning, blastema cell proliferation and cartilage induction during axolotl tail regeneration. Development. 2005; 132:3243–3253. [PubMed: 15983402]

Sellers DL, Maris DO, Horner PJ. Postinjury niches induce temporal shifts in progenitor fates to direct lesion repair after spinal cord injury. J Neurosci. 2009; 29:6722–67333. [PubMed: 19458241]

Shibuya S, Miyamoto O, Itano T, Mori S, Norimatsu H. Temporal progressive antigen expression in radial glia after contusive spinal cord injury in adult rats. Glia. 2003; 42:172–183. [PubMed: 12655601]

Shifman, MI.; Jin, LQ.; Selzer, M. Regeneration in the lamprey spinal cord. In: Becker, CG.; Becker, T., editors. Model organisms in spinal cord regeneration. Wiley-VCH; Weinheim: 2007. p. 229-262.

Silver J, Miller JH. Regeneration beyond the glial scar. Nat Rev Neurosci. 2004; 5:146–156. [PubMed: 14735117]

Simons M, Trotter J. Wrapping it up: the cell biology of myelination. Curr Opin Neurobiol. 2007; 17:533–540. [PubMed: 17923405]

Singer M, Nordlander RTH, Egar M. Axonal guidance during embryogenesis and regeneration in the spinal cord of the newt: the blue print hypothesis of neural pathway patterning. J Comp Neurol. 1979; 185:1–22. [PubMed: 429610]

Sjöstrand, F. Electron microscopy of cells and tissues. Vol. 1. Academic Press; London New York: 1967.

Stensaas, LJ. Regeneration in the spinal cord of the newt. Notopthalmus (Triturus) pyrrhogaster. In: Kao, CC.; Bunge, RP.; Reier, PJ., editors. Spinal cord reconstruction. Raven; New York: 1983. p. 121-149.

Takeda A, Goris RC, Funakoshi K. Regeneration of descending projections to the spinal cord neurons after spinal hemisection in the goldfish. Brain Res. 2007; 1155:17–23. [PubMed: 17493589]

Tanaka EM, Ferretti P. Considering the evolution of regeneration in the central nervous system. Nat Rev Neurosci. 2009; 10:713–723. [PubMed: 19763104]

Tennyson VM. The fine structure of the axon and growth cone of the dorsal root neuroblast of the rabbit embryo. J Cell Biol. 1970; 44:62–79. [PubMed: 5409464]

Thuret S, Moon LD, Gage FH. Therapeutic interventions after spinal cord injury. Nat Rev Neurosci. 2006; 7:628–643. [PubMed: 16858391]

Trujillo-Cenóz O, Fernández A, Radmilovich M, Reali C, Russo R. Cytological organization of the central gelatinosa in the turtle spinal cord. J Comp Neurol. 2007; 502:291–308. [PubMed: 17348014]

Vessal M, Aycock A, Tess Garton M, Ciferri M, Darian-Smith C. Adult neurogenesis in primate and rodent spinal cord: comparing a cervical dorsal rhizotomy with a dorsal column transection. Eur J Neurosci. 2007; 26:2777–2794. [PubMed: 18001275]

Williams RM, Bastiani J, Lia B, Chalupa LM. Growth cones, dying axons, and developmental fluctuations in the fiber population of the cat's optic nerve. J Comp Neurol. 1988; 246:32–69. [PubMed: 3700717]

Wood MR, Cohen MJ. Synaptic regeneration in identified neurons of the lamprey spinal cord. Science. 1979; 206:344–347. [PubMed: 482943]

Zhang F, Clarke JDW, Ferretti P. FGF-2 up-regulation and proliferation of neural progenitors in the regenerating amphibian spinal cord in vivo. Dev Biol. 2000; 225:381–391. [PubMed: 10985857]

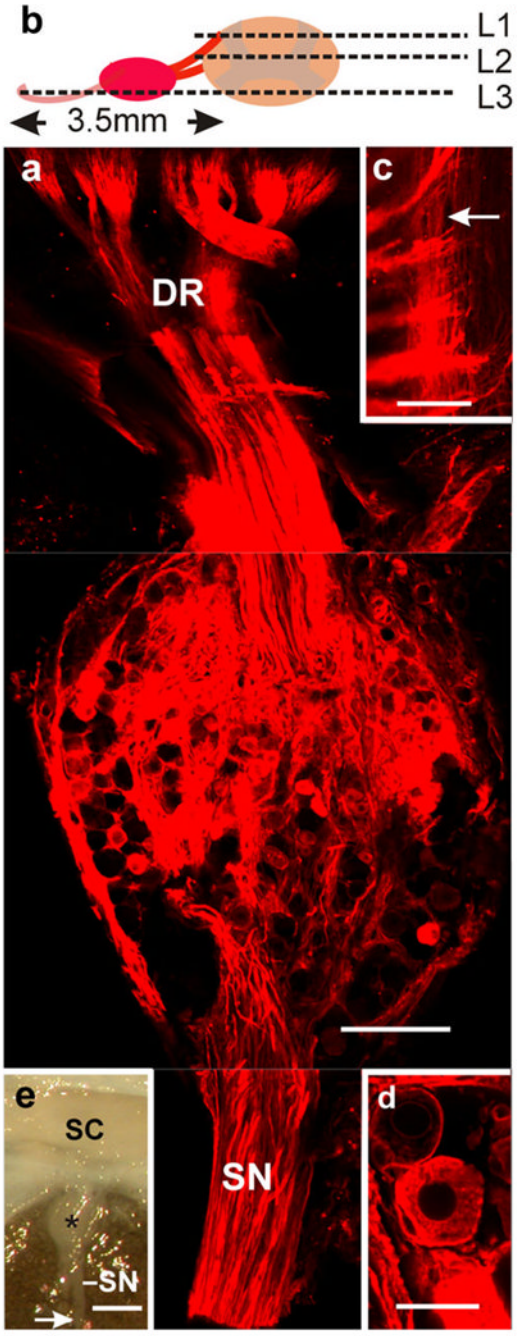

Fig. 1.

Transganglionic labeling of primary sensory fibers. **a** Whole ganglion combining, within a single plane, confocal optical sections taken at levels 1–3 (*L1–L3*) as indicated in **b** (*SN* sensory nerves, *DR* dorsal roots). **c** High magnification view of level 1 illustrating the penetration of dorsal roots into the cord and the distribution of the thinner longitudinally running branches of the sensory axons (*arrow*). **d** Note that the lipophilic dye stains the neural components of the ganglion without spreading into the extracellular space. **e** Macro-image depicting the arrival of the main sensory nerves (*SN*) to a dorsal ganglion (*star*). The *arrow* indicates the site at which the nerves were cut and DiI crystals applied with a

micropipette without spurious contamination of the cord surface (enclosed in the vertebral canal; *SC* spinal cord). *Bars* 250 μm (**a**), 100 μm (**c**), 25 μm (**d**), 1 mm (**e**)

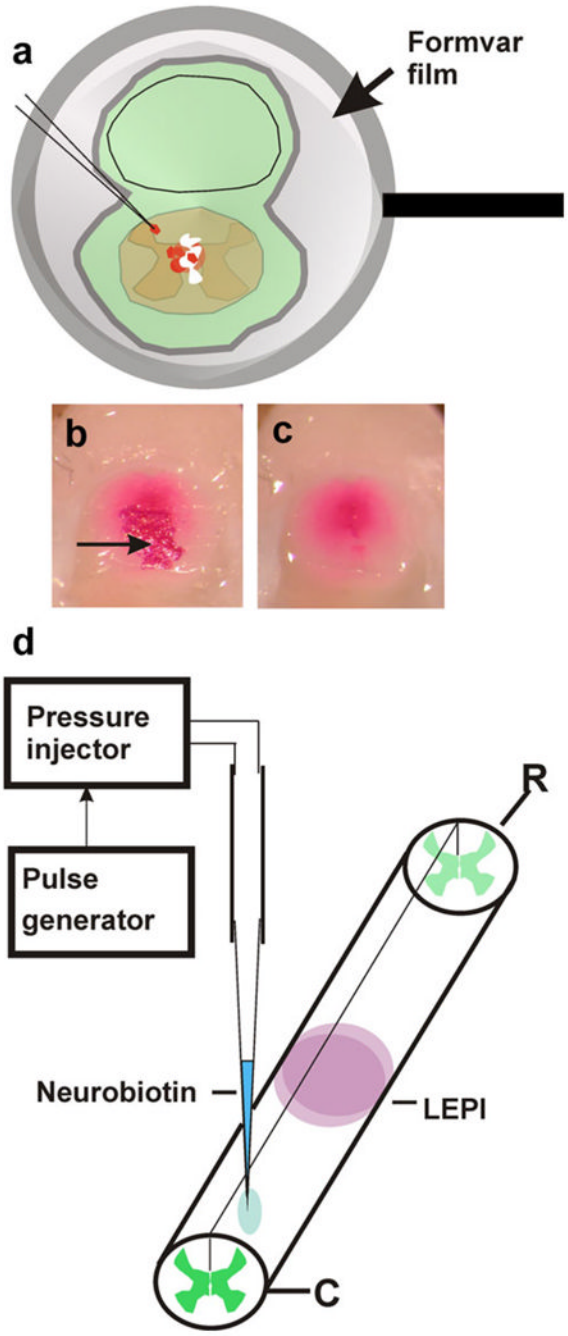

Fig. 2.

Retrograde neuronal labeling. **a** To apply 1,1′, di-octadecyl 1–3,3,3′,3′-tetramethylcarbocyanine perchlorate (DiI) crystals to the cut surface of the cord but to reduce the risk of spurious labeling of neighboring tissues, fixed cords and surrounding tissues were covered with an adhering ultrathin Formvar film supported by Sjöstrand-type metal rings. Small openings were made in the films, and DiI crystals were applied to the film-coated cords. Direct contact between the lipophilic dye and tissues was thus reduced to the area underlying the opening in the film. To avoid dispersion of DiI crystals during incubation, each preparation was coated with a second layer of undamaged film. For embedding and sectioning, dye crystals lying outside the central cord region were removed

together with the film as shown in **b** (before film removal) and **c** (after film removal). The *arrow* in **b** indicates a group of DiI crystals. **d** Neurobiotin injections were performed by pressure-injection with a glass micropipette. The animals were killed 4 days after injection, and the spinal cord was processed as described in Materials and methods (*LEPI* lesion epicenter, *R* rostral, *C* caudal)

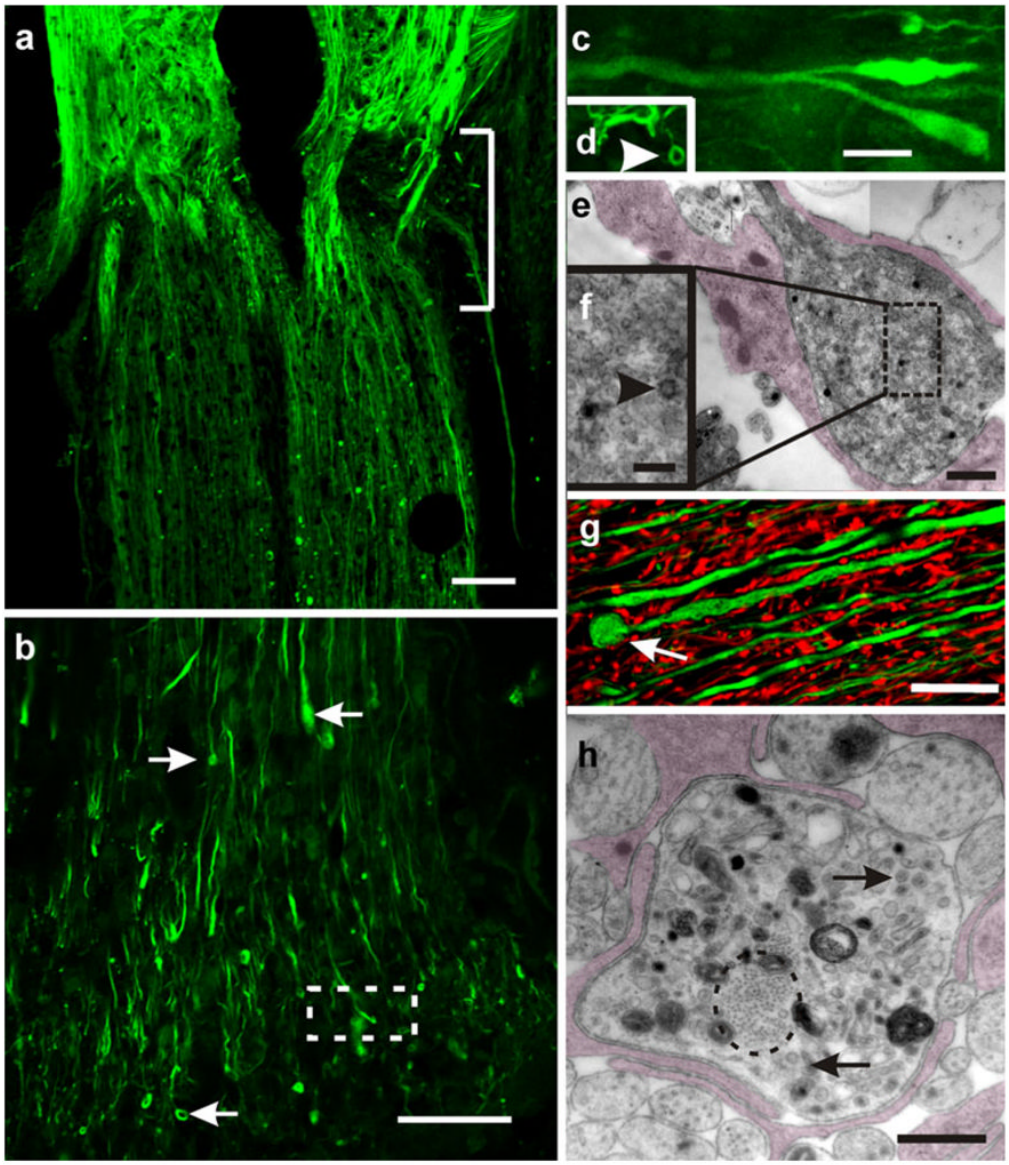

Fig. 3.

Regenerating axons cross the injured site. **a** Longitudinal section of a transected cord 20 days after injury. Regenerating axons stained for Neurofilament M (NF-M; *green*) can be seen crossing the injured site (*bracket*) and invading the caudal stump; confocal optical section. **b** Enlarged view of a bundle of regenerating axons that have penetrated the caudal portion of the cord (*small arrows* enlarged tips and the ring-like endings of regenerating axons); confocal optical section. **c** Area within the *box* in **b** examined at higher magnification. Note the presence of lanceolated and club-like "growth cones" intermingled with small terminal "rings" (*arrowhead* in **d**); confocal optical section). **e** Zone caudal to the injured site. Enlarged axon profiles identified as growth cones containing clusters of small vesicles; collage of two images obtained by transmission electron microscopy (TEM). The growth cone appears partially covered by glial processes (*shadowed*). The *box* is shown in **f** at a higher magnification. Note the presence of a characteristic "coated vesicle" (*arrowhead*). **g** "Retraction balls" or dystrophic end bulbs appear spherical (*arrow*) and are usually larger than the growth cones; stack of five confocal optical sections. Double-

immunostaining with NF-M (*green*) and glial fibrillary acidic protein (GFAP; *red*). **h** TEM image showing a cross section passing through a dystrophic end bulb. Note the presence of a bundle of neurofibrils (*encircled*), mitochondria, cumuli of large vesicles (*arrows*), and dense bodies with the aspect of phagosomes. The ending is partially covered by glial lamellae (*shadowed*). *Bars* 200 μm (**a**), 100 μm (**b**), 5 μm (**c**, **d**), 0.5 μm (**e**), 100 nm (**f**), 20 μm (**g**), 1 μm (**h**)

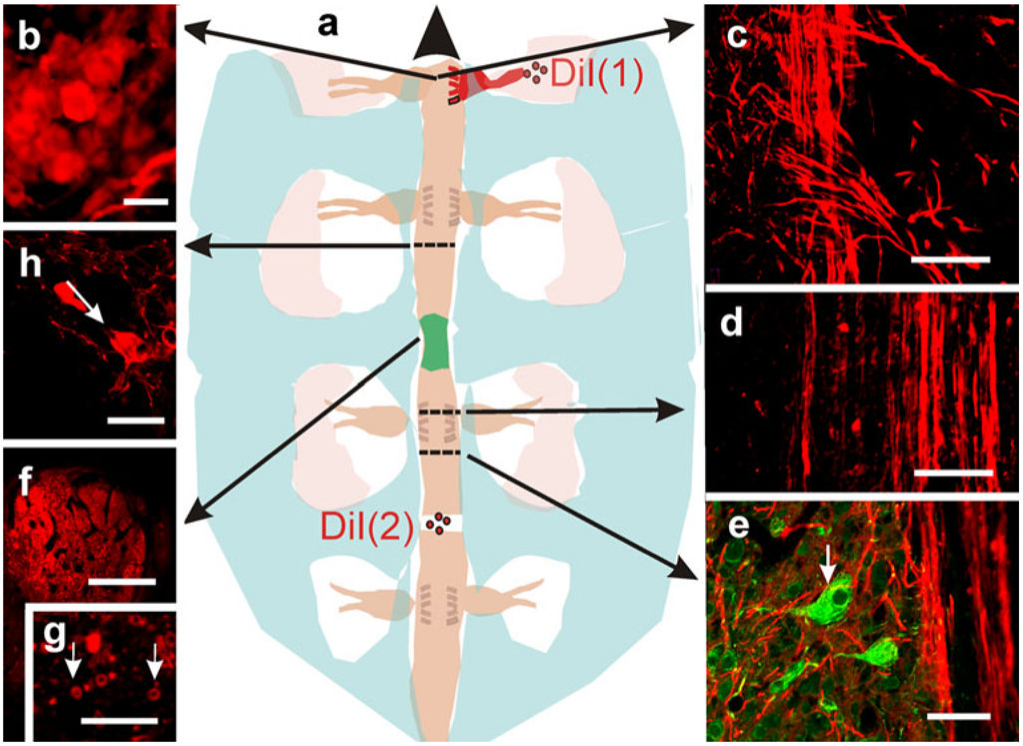

Fig. 4.

Origin of regenerating axons. **a** Representation depicting two different experiments with DiI as an axonal marker (*long arrows* correlation of the topology of the microscopic images with the gross anatomy of the cord; *large arrowhead* rostral). In one experiment (*DiI (1)*), crystals of the dye were applied to sectioned sensory nerves entering into a dorsal root ganglion at one side of the injured cord and lying cephalic with respect to the lesion epicenter (*shadowed green*). **b** Stained neurons in the ganglion (epifluorescence microscopy). **c** Sensory axons entering the dorsal horns. **d**, **e** Confocal optical sections revealing the occurrence of stained axons that have crossed the lesion site and have ramified close to neuronal bodies (*arrow* in **e**; DiI+NF-M). **f** When dye crystals were applied to the cut surface of the cord, caudal to the lesion site, conspicuous bundles of stained axons were detected at the bridge level; confocal optical section. **g** Higher magnification view of myelinated axons crossing the bridge; confocal optical section. **h** The parent neurons of some of the crossing axons (*arrow*); confocal optical section. *Bars* 10 μm (**b**, **f**, **g**), 30 μm (**d**), 40 μm (**e**), 50 μm (**h**), 100 μm (**c**)

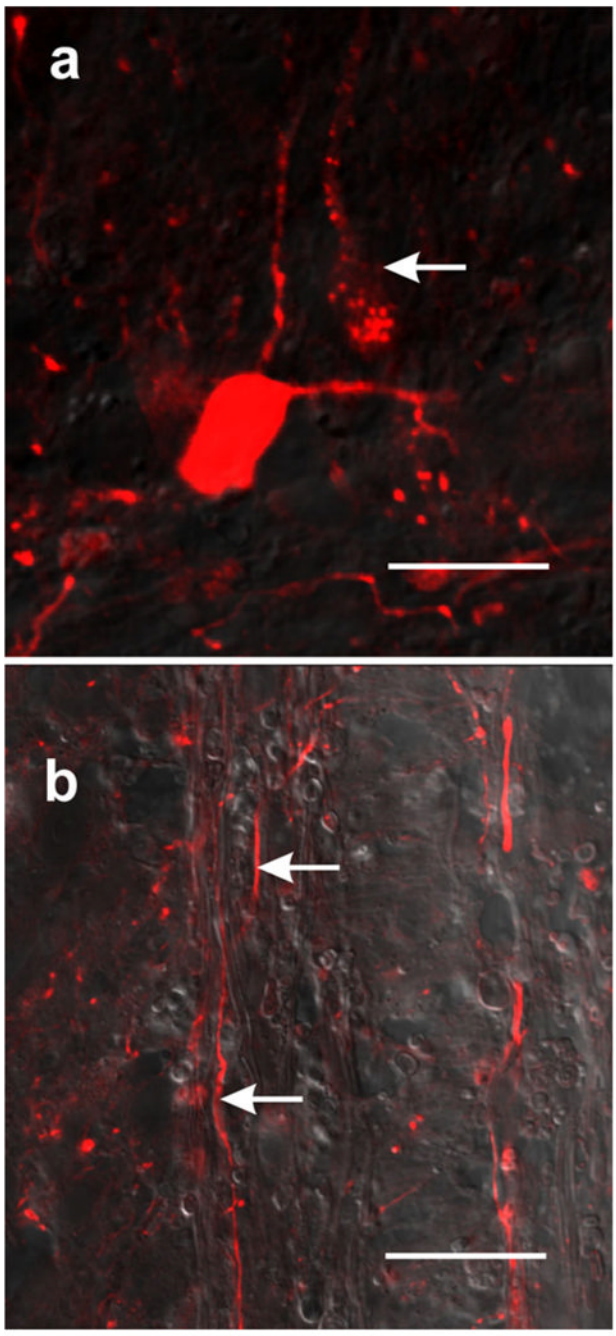

Fig. 5.
Retrograde labeling with neurobiotin reveals neurons and neural processes in the rostral stump. **a** One neuron appears to be Golgi-like stained, whereas another one only shows small fluorescent granules distributed in the perikaryon and main process (*arrow*); confocal optical section. **b** Neural processes also appear to be Golgi-like stained in the bridge zone (*arrows*); trans-illuminated confocal optical section. *Bars* 10 μm

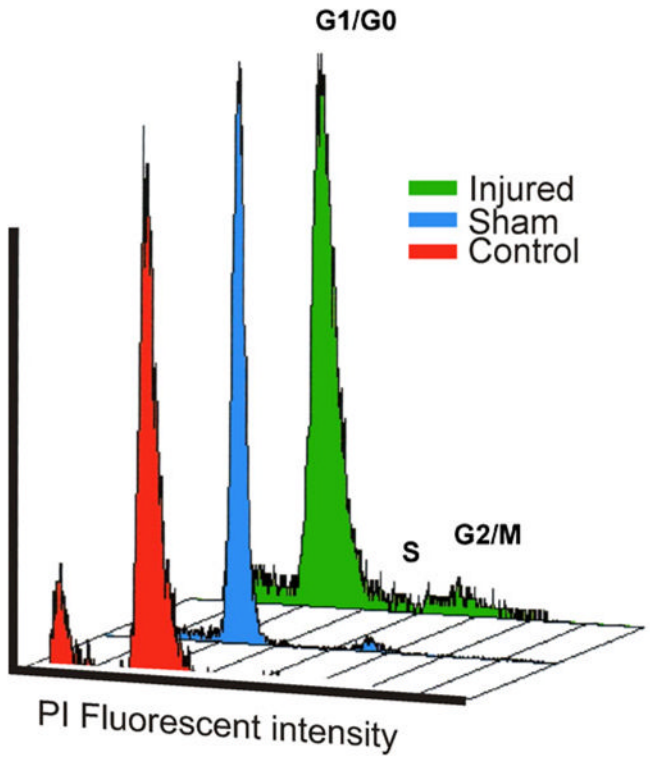

Fig. 6.

Spinal cord transection increases cell proliferation. DNA content histograms (FL2-A) obtained by flow cytometry showing G1/G0, S, and G2/M cell cycle stages corresponding to propidium iodide (*PI*)-stained spinal cord cells from injured, sham-operated, and control turtles. Cells from the injured cords were obtained from the portion containing the lesion epicenter. Data from sham and control experiments were collected from homologous spinal cord segments. Note the higher proliferation rate (S-G2/M) of cells from the injured region. Differences were statistically significant ($P<0.05$, one-sided Wilcoxon rank-sum test; see also Table 2)

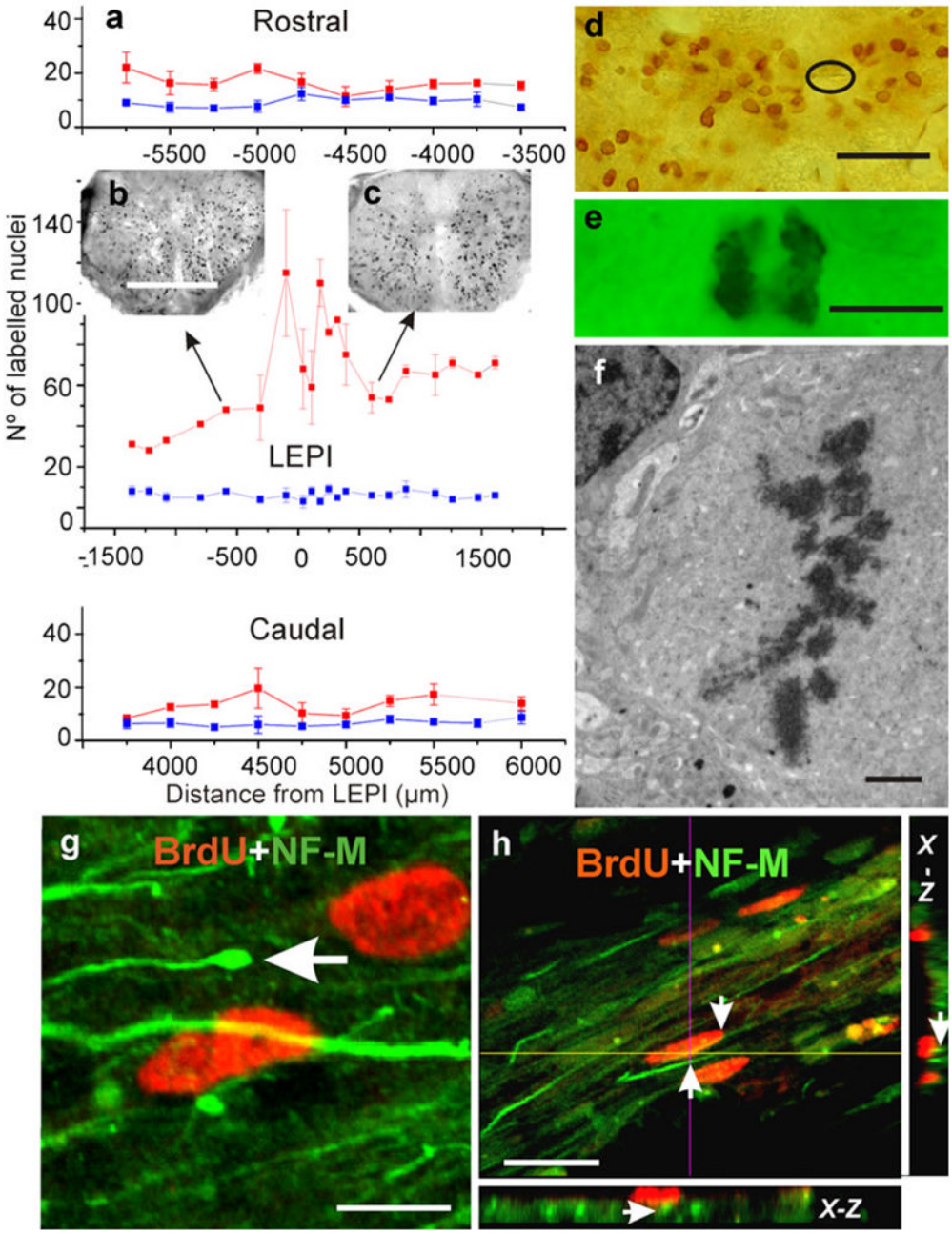

Fig. 7.

Spinal cord injury increases cell proliferation. **a** Mean number of BrdU-positive nuclei ± the standard deviation plotted against distance (in μm) from the lesion epicenter (*red line*, *LEPI*) and corresponding segment in control animals (*blue line*). Note that this is a single plot divided into three sequential rostro-caudal portions (*negative numbers* progression toward more cephalic segments). **b**, **c** Two small spinal cord images showing the distribution of BrdU-positive nuclei at two levels of the cord (*arrows*). **d** Even though BrdU-positive nuclei were found in all areas of the cord, they appeared concentrated near the reduced central canal (*encircled*). **e** Mitotic figures were usually found together with BrdU-positive nuclei; transmission light microscopy. **f** TEM image of cell in meta-phase; injured but not BrdU-injected material. **g**, **h** Double-labeling experiments revealed a close association between

cells with BrdU-positive nuclei and the bundles of regenerating axons that expressed NF-M and that crossed the lesion site (arrow in **g** enlarged distal portion of a regenerating axon). **h** Proximity of two NF-M-positive axons to a BrdU-positive nucleus (*arrows* in **h**); planes obtained across a stack of 20 optical sections (*x-z* orthogonal plane). *Bars* 300 μm (**b**), 30 μm (**d**), 5 μm (**e**), 2 μm (**f**), 5 μm (**g**), 20 μm (**h**)

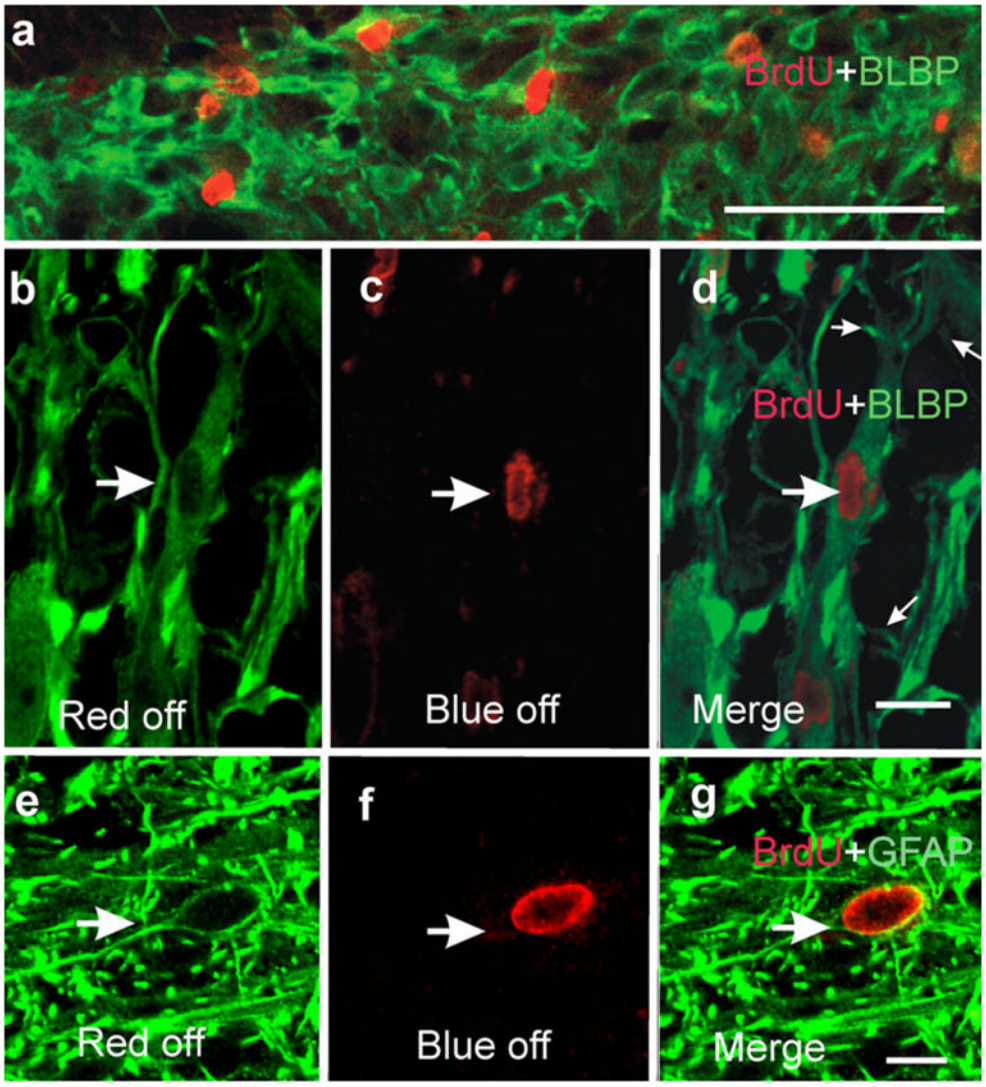

Fig. 8.

Cycling cells express glial markers. **a** Low power confocal microscope image (stack of five optical sections) showing several brain lipid-binding protein (BLBP)-expressing cells with their nuclei labeled with BrdU (note the random cellular organization). **b**–**d** High magnification images demonstrating that some cells expressing BLBP have BrdU-labeled nuclei (*large arrows*). **d** Merged image (*small arrows* main processes arising from the elongated cell body); confocal optical section. **e**–**g** Immunohistochemistry against GFAP showing abundant fibers surrounding a BrdU-positive nucleus; confocal optical section. **g** Merged image showing that the BrdU-positive nucleus pertains to a GFAP-positive cell. *Bars* (only shown in **a**, **d**, **g**) 50 μm (**a**), 10 μm (**b**–**g**)

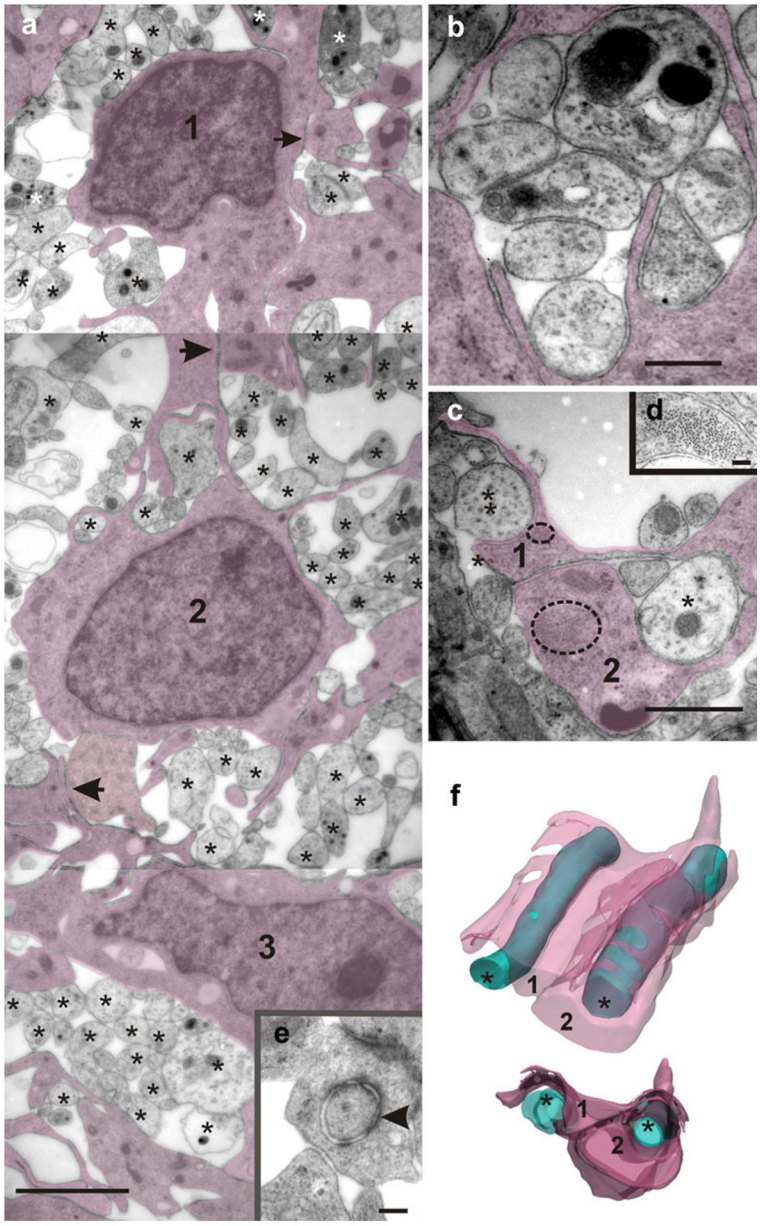

Fig. 9.

The bridge region is characterized by a loose embryonic-like cellular organization. **a** Panoramic TEM image showing three cells (*1*, *2*, *3*, *shadowed*) sending processes that partially cover numerous regenerating axons of uneven size (*stars*). Note the close intercellular contacts without visible membrane specializations (*arrows*). Desmosome-like contacts also occur in this region (see *arrowhead* in **e**). **b** Higher magnification electron micrograph showing a group of axons completely surrounded by glial processes (*shadowed*). **c** Two axons crossing the bridge (*stars*) were serially followed (25 serial sections) to explore their spatial relationships with adjacent glial processes (*1*, *2*). Two bundles of gliofibrils have been *encircled*, one being shown at higher magnification in **d. f** The resulting three-dimensional (3D) models displayed from two different points of view reveal that the axon *left* in **c** is partially covered by a glial lamella (*1*), whereas the axon *right* in **c** is completely

ensheated by glial lamellae *1* and *2*. *Bars* 2 μm (**a**), 160 nm (**e**), 0.5 μm (**b**), 1 μm (**c**), 80 nm (**d**)

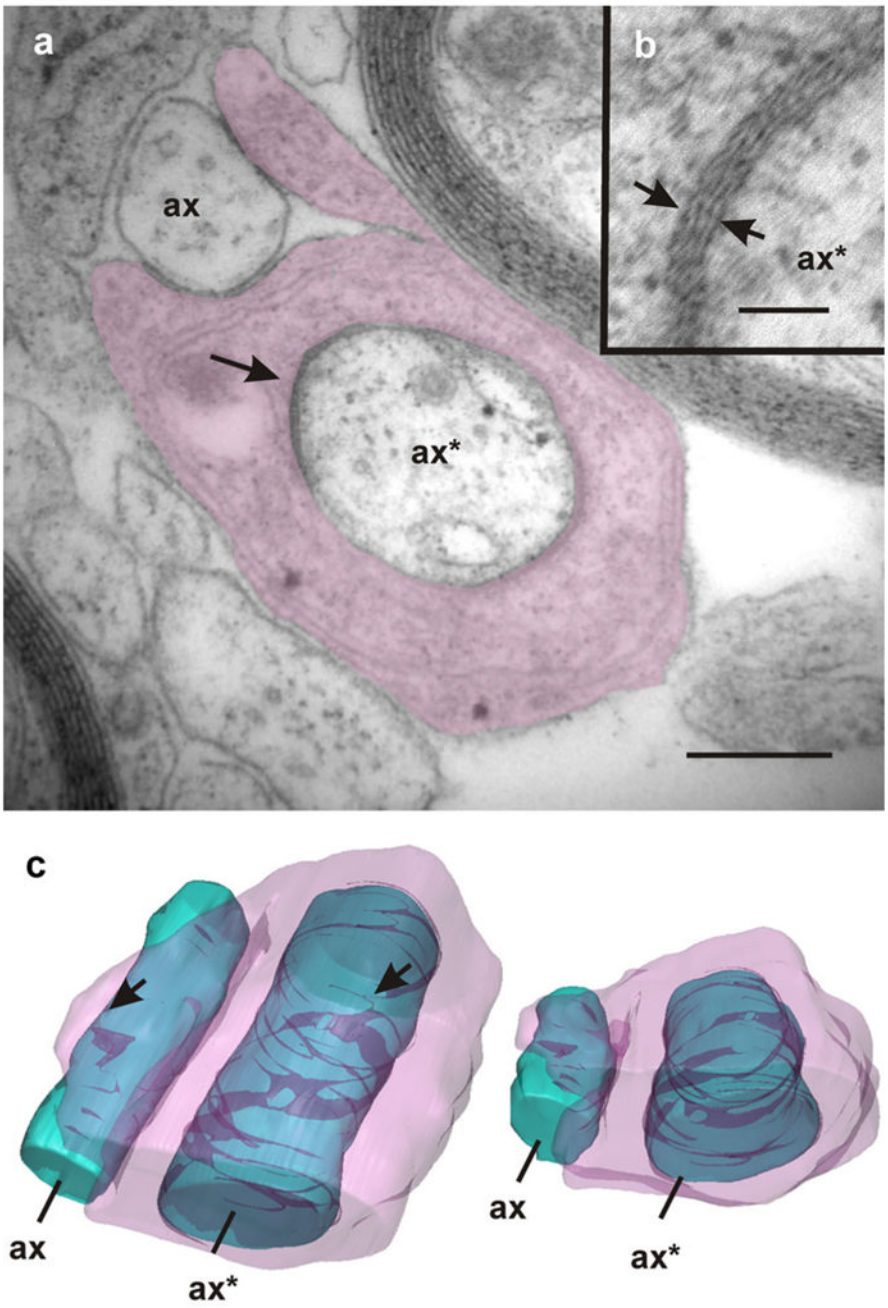

Fig. 10.

Ensheathing of regenerating axons. Intermixed with axons that appear partially ensheathed (*ax*) lie axons (*ax**) that are completely enveloped by processes of glial cells (*shaded*). Note the presence of zones in which the periaxonal space is extremely reduced exhibiting an increased electron density (*arrows* in **a**, **b**). The TEM image corresponds to section number 12 of a continuous series comprising 17 sections. The accompanying 3D models (**c** frontal and dorsal views) reveal that these close junctions form discontinuous helical bands along the periaxonal space (*arrowheads*). *Bars* 1 μm (**a**), 80 nm (**b**)

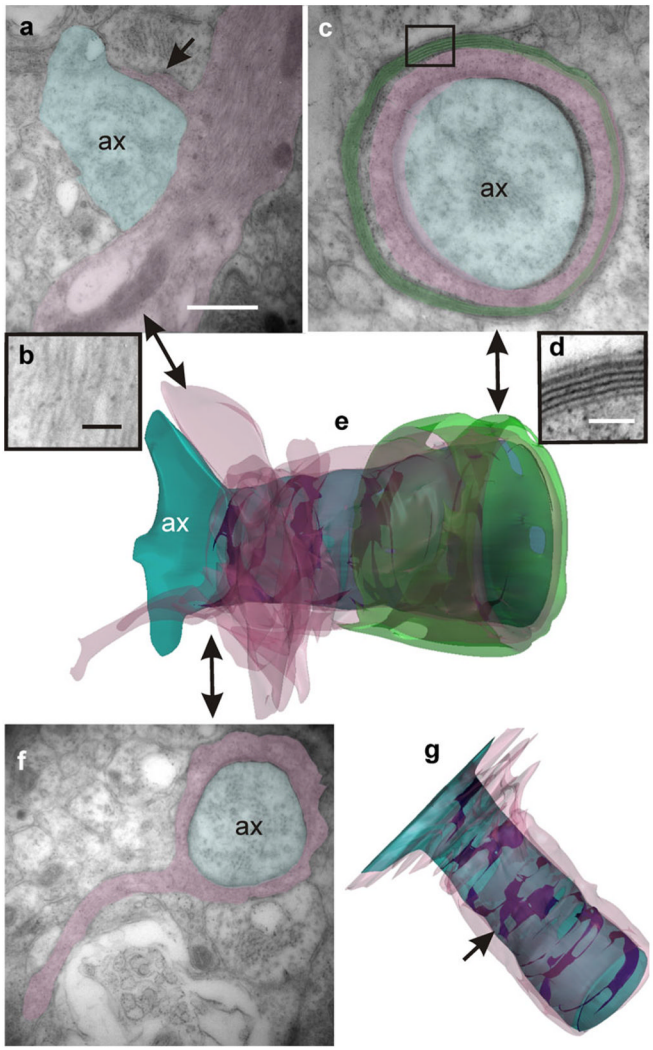

Fig. 11.

Example of a 3D reconstruction of an axon sheath (*large double-headed arrows* correspondence between the 3D model and TEM images). The 3D model in **e** represents a short axon segment with a heterogeneous glial sheath (*blue* axon, *pink* glial covering, *green* myelin). The reconstruction results from computer processing of 22 serial TEM images. **a** The naked axon (*ax*) begins to be enveloped by a short lamella (*arrow*) stemming from a glial prolongation containing gliofibrils (shown in **b** at higher magnification). **f** Advancing through the serial sections, a level is attained at which the glial ensheathing becomes complete, but myelin is still absent. **c**, **d** Finally, the enveloping cell produces the typical, regularly spaced, myelin sheaths. **g** Upper view of the 3D model in which the myelin covering has been omitted. Note the helical bands (*arrow*) corresponding to the electron-dense axon-glial junctions. *Bars* 0.5 μm (**a**, **c**, **f**), 100 nm (**d**), 80 nm (**b**)

Table 1

Primary antibodies used in this study

Antigen	Immunmogen	Manufacturer	Dilution
Bromodeoxyuridine (BrdU)	BrdU conjugated to bovine serum albumin	Dakocytomation (Denmark), mouse monoclonal, cat. no. M0744, lot no. 00004862	1:500
Brain lipid-binding protein (BLBP)	Recombinant whole BLBP	Chemicon (Temecula Calif., USA), rabbit polyclonal, cat. no.AB 9558, lot no. 6080037568	1:1000
Glial fibrillary acidic protein (GFAP)	GFAP purified from human brain	Sigma-Aldrich (St. Louis, Mo., USA), rabbit polyclonal, product no. G9269, lot no. 066K4838	1:500
	GFAP purified from pig spinal cord	Sigma-Aldrich, mouse monoclonal, product no. G3893, lot no. 037K4759	1:500
Neurofilament M (NF-M)	Recombinant fusion protein containing the C-terminal 168 amino acids of rat neurofilaments	Chemicon, rabbit polyclonal, cat. no. AB1987, lot no. 18030413	1:500
Anti-human neuronal protein	RNA-binding protein of the embryonic lethal abnormal visual (Elav) family from mouse	Molecular Probes (Eugene, Ore., USA), mouse monoclonal, cat. no. 21275, lot no. A21275	1:100

Table 2

Values of flow cytometry cell cycle analyses of proliferating (S-G2/M) cells stained with propidium iodide. The samples were obtained from control, sham-injured, and injured spinal cord segments. Mean±standard deviation values are indicated in *bold*. Note that mean values of uninjured and control sham spinal cord segments are significantly different from those obtained from injured spinal cords ($P<0.05$, as determined by one-sided Wilcoxon rank-sum test)

Sample	% Proliferation (S/G2-M)
Uninjured spinal cord (*n*=3)	3.92
	4.30
	2.89
	3.70±0.5
Control sham (*n*=3)	2.75
	2.62
	1.78
	2.38±0.53
Injured spinal cord (*n*=3)	9.07
	8.94
	9.68
	9.23±0.4